



**HAL**  
open science

## Organic photo sensors for multi-angle light scattering characterization of particle systems

Matthias Sentis, Fabrice R.A. Onofri, Olivier Dhez, Jean-Yves Laurent,  
Fabien Chauchard

► **To cite this version:**

Matthias Sentis, Fabrice R.A. Onofri, Olivier Dhez, Jean-Yves Laurent, Fabien Chauchard. Organic photo sensors for multi-angle light scattering characterization of particle systems. *Optics Express*, 2015, 23 (21), pp.27536. 10.1364/OE.23.027536 . hal-02373582

**HAL Id: hal-02373582**

**<https://hal.science/hal-02373582>**

Submitted on 21 Nov 2019

**HAL** is a multi-disciplinary open access archive for the deposit and dissemination of scientific research documents, whether they are published or not. The documents may come from teaching and research institutions in France or abroad, or from public or private research centers.

L'archive ouverte pluridisciplinaire **HAL**, est destinée au dépôt et à la diffusion de documents scientifiques de niveau recherche, publiés ou non, émanant des établissements d'enseignement et de recherche français ou étrangers, des laboratoires publics ou privés.

# Organic photo sensors for multi-angle light scattering characterization of particle systems

Matthias Sentis,<sup>1</sup> Fabrice R.A. Onofri,<sup>1,\*</sup> Olivier Dhez,<sup>2</sup> Jean-Yves Laurent,<sup>3</sup> and Fabien Chauchard<sup>4</sup>

<sup>1</sup> Aix-Marseille Université, CNRS, IUSTI, UMR 7343, 13453 Marseille Cedex 13, France

<sup>2</sup> ISORG, MINATEC, 38040 Grenoble Cedex 09, France

<sup>3</sup> LITEN, CEA Grenoble, 38054 Grenoble Cedex 9, France

<sup>4</sup> INDATECH, 34 830 Clapiers, France

\*[fabrice.onofri@univ-amu.fr](mailto:fabrice.onofri@univ-amu.fr)

**Abstract:** Organic Photo Sensor (OPS) technology allows printing on conformable plastic-like substrates complex-shaped, arbitrarily-sized and pre-aligned photosensitive elements. This article reports, to the best of our knowledge, the first investigation to implement this emerging technology for Multi-Angle Light Scattering (MALS) characterization of nano- and microparticle suspensions. Monte Carlo and Lorenz-Mie theory calculations as well as preliminary experimental results on latex suspensions clearly demonstrate the potential of the proposed approach.

**OCIS codes:** (290.5850) Scattering, particles, (280.2490) Flow diagnostics, (120.3930) Metrological instrumentation, (040.5160) Photodetectors

---

## References and links

1. R. Xu, *Particle characterization : Light scattering methods* (Kluwer Academic Publishers, 2001).
  2. K. Knobelspiesse, B. Cairns, M. Mishchenko, J. Chowdhary, K. Tsigaridis, B. van Dienenhoven, W. Martin, M. Ottaviani, and M. Alexandrov, "Analysis of fine-mode aerosol retrieval capabilities by different passive remote sensing instrument designs," *Opt. Express* **20** (19), 21457-21484 (2012).
  3. F. R. A. Onofri, M. Wozniak, and S. Barbosa, "On the Optical Characterisation of Nanoparticles and their Aggregates in Plasma Systems," *Contrib. Plasm. Phys.* **51**(2-3), 228-236 (2011).
  4. M. G. Heffels, R. Polke, M. Radle, N. Sachweh, M. Schafer, and N. Scholtz, "Control of Particulate Processes by Optical Measurement Techniques," *Part. Part. Syst. Charact.* **15**(5), 211-218 (1998).
  5. M. Giacomelli, Y. Zhu, J. Lee, and A. Wax, "Size and shape determination of spheroidal scatterers using two-dimensional angle resolved scattering," *Opt. Express* **18**(14), 14616-14626 (2010).
  6. N. Roth, K. Anders, and A. Frohn, "Refractive index measurements for the correction of particle sizing methods," *App. Opt.* **30**(33), 4960-4965 (1991).
  7. S. Gao, J. Shen, J. C. Thomas, Z. Yin, X. Wang, Y. Wang, W. Liu, and X. Sun, "Effect of scattering angle error on particle size determination by multiangle dynamic light scattering," *Appl. Opt.* **54**(10), 2824-2831 (2015).
  8. P. J. Wyatt, K. L. Schehrer, S. D. Phillips, C. Jackson, Y.-J. Chang, R. G. Parker, D. T. Phillips, and J. R. Bottiger, "Aerosol particle analyzer," *Appl. Opt.* **27**(2), 217-221 (1988).
  9. H. Oltmann, J. Reimann, and S. Will, "Single-shot measurement of soot aggregate sizes by wide-angle light scattering (WALS)," *Appl. Phys. B* **106**(1), 171-183 (2012).
  10. P. N. Pusey, "Suppression of multiple scattering by photon cross-correlation techniques," *Curr. Opin. Colloid Interface Sci.* **4**, 177-185 (1999).
  11. I. D. Block, and F. Scheffold, "Modulated 3D cross-correlation light scattering: Improving turbid sample characterization," *Rev. Sci. Instrum.* **81**, 123107 (2010).
  12. ISORG, "Organic Photodetectors and Large Area Photosensors," (September, 2015), <http://www.isorg.fr>.
  13. J. M. Verilhac, "Recent developments of solution-processed organic photodetectors," *Eur. Phys. J. Appl. Phys.* **63**, 14405 (2013).
  14. G. Azzellino, A. Grimoldi, M. Binda, M. Caironi, D. Natali, and M. Sampietro, "Fully Inkjet-Printed Organic Photodetectors with High Quantum Yield," *Adv. Mater.* **25**(47), 6829-6833 (2013).
  15. M. Young, "Pinhole Optics," *Appl. Opt.* **10**(12), 2763-2767 (1971).
  16. P. Martinez-Vara, J. Silva Barranco, S. I. De Los Santos G, J. Munoz-Lopez, M. A. Torres-Rodriguez, R. Suarez Xique, and G. Martinez-Niconoff, "Diffraction by three-dimensional slit-shape curves: decomposition in terms of Airy and Pearcey functions," *Opt. Lett.* **40**(15), 3496-3499 (2015).
-

17. C. Calba, L. Mèès, C. Rozé, and T. Girasole, "Ultrashort pulse propagation through a strongly scattering medium: simulation and experiments," *J. Opt. Soc. Am. A* **25**(7), 1541-1550 (2008).
18. O. Glatter, "Static light scattering of large systems," in *Neutron, X-rays and Light. Scattering Methods Applied to Soft Condensed Matter*, Th. Zemb and P. Lindner, eds. (Elsevier, 2002).
19. F. R. A. Onofri, S. Barbosa, O. Touré, M. Woźniak, and C. Grisolia, "Sizing highly-ordered buckyball-shaped aggregates of colloidal nanoparticles by light extinction spectroscopy," *J. Quant. Spectr. Rad. Transfer* **126**, 160-168 (2013).
20. R. K. Chakrabarty, N. D. Beres, H. Moosmüller, S. China, C. Mazzoleni, M. K. Dubey, L. Liu, and M. I. Mishchenko, "Soot superaggregates from flaming wildfires and their direct radiative forcing," *Sci. Rep.* **4**, 5508 (2014).
21. D. Lottin, D. Ferry, J. M. Gay, D. Delhaye, and F. X. Ouf, "On methods determining the fractal dimension of combustion aerosols and particleclusters," *J. Aerosol Sci.* **58**, 41-49 (2013).

## 1. Introduction

There are many different types of MALS systems for the determination of size and concentration of nano to microparticle suspensions and aerosols [1-3]. However, there are typically two types: those that use a single photodetector (e.g., a standardized avalanche photodiode or photomultiplier) rotating around the particle sample (e.g., [1-5]) and those using a set of silicon photodiodes (or in some cases, a CCD camera and a specific optics) positioned around or one side of the sample (e.g., [1-3, 6-9]). In the first type, a high angular resolution is achievable and some effects of multiple scattering can be corrected (e.g., [10,11]), but the sample properties must be perfectly constant during the course of the analysis. In the second type, transient suspensions and aerosols may be studied, but the angular resolution obtained is usually limited (e.g., typically a few tens of photodiodes distributed over 0-180° within the scattering plane). Despite the fact that the second systems are probably the most effective and versatile, they require the building of a complex optical bench to support and align all of the components (e.g., lenses, filters, fibers, special mirrors, etc.). Thus, the *a posteriori* optimization or modification of such systems, to characterize different particle systems, is particularly difficult and costly.

As alternatives to the aforementioned problems, this article reports a new approach taking advantage of organic printed electronic technology. In the following, for clarity, we begin with a brief description of the OPS technology and the first prototype developed. Then, we describe our optimization procedure and preliminary results confirming the potential of this totally new approach.

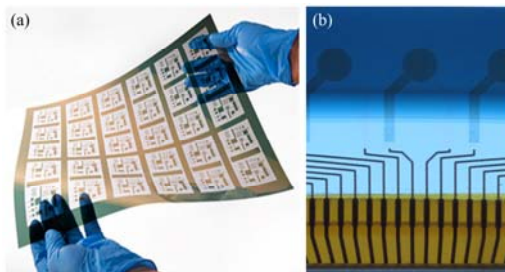


Fig. 1. Photographs of a (a) conventional OPS film and (b) zoom in of simply-shaped photosensitive areas (i.e., darker circular disks below the blue protective coating) [12, 13].

## 2. Experimental set-up

Conventional OPS plastic-like films (or 'foils') developed by ISORG [12], a spin-off from CEA-LITEN, are depicted in Fig. 1. The polyethylene terephthalate (PET) film can be as large as 320 mm x 380 mm for a thickness of less than 300  $\mu\text{m}$ . Several tens to hundreds of photosensitive elements (i.e., OPS) can be printed on it *via* an inkjet-like process [12-14]. The film can be bent (i.e., 'conformable') down to a curvature radius of a few centimeters without significant performance losses. The OPSs can be operated in either the photovoltaic (zero bias) or photoconductive (reverse bias) mode [1]. The basic photosensitive and electronic

characteristics of the OPSs are comparable to silicon technology in terms of quantum efficiency (more than 55% in the visible range) or noise-equivalent power, but they are still lacking in terms of the intrinsic response time (e.g., tens of milliseconds, instead of nanoseconds), spectral range (e.g., 350-700 nm, instead of 300-1100 nm) and durability [13].

A schematic and a photograph of the first prototype of particle sizing instrument based on OPS technology are shown in Figs. 2(a) and 3(b) respectively. All of the optical components are embedded in a cylindrical and metallic casing (internally black-anodized) with an external radius of 140 mm, see Fig. 2(b). In the present study, the particle sample to be analyzed is simply placed in a cylindrical light scattering cuvette (cell in Suprasil quartz). The cuvette, with internal and external radii  $R_{C1}$  and  $R_{C2}$  respectively, is located at the center of the instrument. The parallel or perpendicularly polarized laser beam of a 1 W YAG Diode-pumped solid-state laser (DPSS), with wavelength  $\lambda=532$  nm, is focused at the center of the cuvette down to a waist diameter of  $2\omega_0=200$   $\mu\text{m}$ . For extinction measurements, this prototype uses a conventional collection optics and avalanche photodiode (APD).

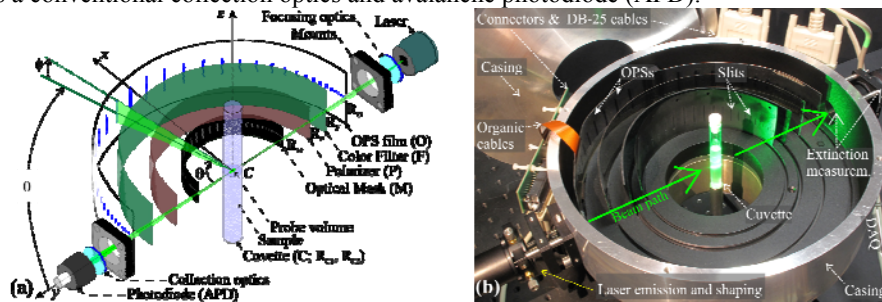


Fig. 2. (a) Schematic and (b) photograph of a MALS system prototype taking advantage of OPS technology (40 curved photosensitive elements distributed over  $\approx 1^\circ$  to  $179^\circ$ ).

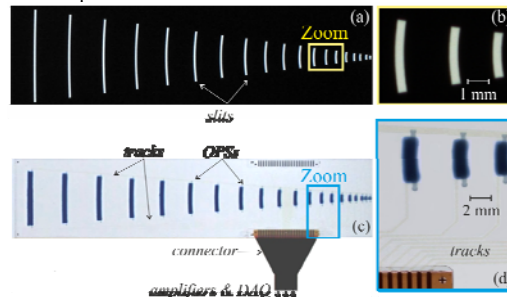


Fig. 3. (a-b) Shadowgraph images of half of the unfold optical mask and (c-d) transmission images of half of the unfold OPS film (the contrast and colors are adjusted for clarity). The width of all OPS (1mm) and all slits (0.5 mm) are constant in contrary to their heights (see Fig. 4 and Visualization 1).

In Figure 2, the film closest to the particle sample is an optical mask, with radius  $R_M$ . It is composed of a thin and black anodized metallic film with  $N_D$  curved slits. These slits, which act as individual pinholes [15, 16], are used to define and limit the angle of view of each OPS (i.e. collection aperture angle). The fact is that, with conformable OPS film, the use of rigid optics (e.g. conventional glass lenses) would be meaningless. In practice, this optical mask is produced with a high precision surface-mounting technology that is traditionally used for producing electronic circuits. The path of the light scattered by the sample in the direction defined by the scattering angle range  $\theta \pm \delta\theta$  and azimuth angle range  $\phi \pm \delta\phi$  is illustrated in Fig. 2(a). The light, scattered by the particles within the optical probe volume, passes through the slits prior to reach the OPSs. The second polymer film is a dichroic linear-polarizer (either parallel or perpendicular), with radius  $R_P$ . The third film, with radius  $R_F$  is a polymer band-pass color filter, nearly centered on the laser wavelength. The farthest film, with radius  $R_O$ , is

the OPS one. The shape of each of the  $N_D$  photosensitive elements is homothetic to the corresponding curved slit (i.e., placed in front). The total unfolded dimensions of the optical mask and the OPS films of the prototype shown in Fig. 3 are  $L \times H=214 \times 42$  mm and  $L \times H=390 \times 42$  mm, respectively. The curvature radii (i.e. distance from the optical probe center) of the four films are  $R_M=67$ ,  $R_P=80$ ,  $R_F=100$  and  $R_O=124$  mm. With  $R_{C1}=4$ mm and  $R_{C2}=4.5$ mm, as well as slits width (0.5 mm) and OPS width (1mm), these characteristics dimensions allow achieving an angular resolution on the scattering angle of  $\delta\theta=\pm 0.5^\circ$  for all of the  $N_D=40$  photosensitive elements distributed over the scattering angle range of  $\theta=1-179^\circ$ .

Fig. 3 shows a shadowgraph image of half of the optical mask (i.e., opaque metallic plate) and a transmission image of half of the OPS film (i.e., mostly transparent). Zoomed in areas of the corresponding 7th to 9th photosensitive elements ( $\theta_7=10.5^\circ$ ,  $\theta_8=13^\circ$  and  $\theta_9=16^\circ$ ) are also shown. The multi-wire planar cables that are in orange in Fig. 2(b) ensure the electrical connection (not yet optimized) between the tracks of the OPS film and conventional metallic connectors and DB-25 cables used by the amplification and the data acquisition (DAQ) electronics. Currently, the OPSs are simply operated in the photovoltaic mode. Similar to silicon photodiodes, the nano currents they deliver are amplified and converted *via* linear transimpedance amplifiers (20 current/voltage multiboard amplifiers from Scitech Instruments Ltd). Note that the moderate conversion rate ( $10^3$  V/A) achieved with the electronics of this first prototype explains why a powerful DPSS laser is necessary. The DAQ is a typical multichannel (no multiplexing) 16-bit resolution system from National Instruments. Its total sampling rate of 250 kS/s, which is much superior to the equivalent response time of the OPS, is used for data averaging and signal-to-noise ratio improvement.

### 3. Optimization procedure

The optimization of the optical setup is performed with geometrical considerations, as well as Lorenz-Mie Theory (LMT, e.g. [1]) and Monte Carlo simulations (e.g. [17]). The Monte Carlo code specifically developed for this study is tridimensional and accounts for most of the parameters of the system, like the shape of the OPS and curved slits, the laser beam intensity profile and polarization, the cuvette and the particle sample scattering properties, etc.

Three main objectives were pursued during the optimization procedure: (i) to maximize the number of photosensitive elements on a given OPS film; (ii) to enhance the local angular resolution of the system and to compensate for the excessive dynamic range of the optical signals collected in the forward and backward scattering regions; (iii) to obtain scattering diagrams that are as close as possible to those predicted by the LMT (in the far-field and in the absence of a cuvette). The latter objective is important because MALS analyses require the solving of an inverse problem and thus, intensive light scattering calculations. The fact is that if the LMT doesn't account for the presence of a cuvette or pinhole optics for instance, it is several orders of magnitude faster than Monte Carlo calculations.

To illustrate our optimization procedure, Fig. 4(a) shows a conditional map of the light intensity that could be measured by an OPS film with infinite spatial resolution and that is set behind the optical mask shown in Fig. 3(a). The results are point-to-point normalized to be independent of the particle scattering properties. The color coding of this Monte Carlo simulation highlights three regions. In the dark regions, no light (i.e., rays in the Monte Carlo framework) passes through the curved slits. The red regions correspond to light rays that pass through the curved slits but which do not meet the required angular resolution. These ring-shaped regions are usually referred to as 'halos'. Indeed, their angular width is the first limiting factor when attempting to maximize the number of independent OPS (i.e., without cross-talking) in the scattering plane. The second main limiting factor is the minimum characteristic dimension ( $\approx 1$  mm) for a photosensitive element that can be printed with the actual technology. The green coding in Fig. 4(a) identifies the regions on the OPS film where the collected rays meet the desired angular criteria, i.e. all rays collected by the  $j$ th OPS (i.e., green region) are scattered by the particle suspension in the expected scattering angular range (i.e.,  $\theta_j \pm \delta\theta$  for  $j=1,2,\dots,N_D$ ). These green regions, identifying the "optimal OPS shapes" for

spherical particles, are roughly in the form of the intersection of a thick circular cone (due to the particle scattering properties) with a right circular cylinder (due to the curvature of the OPS film). Changes in their heights (i.e. azimuthal angle  $\phi$ ) are the result of false-reflection and total internal reflection effects induced by the cuvette walls (e.g. [18]). The white lines signify the upper and lower boundaries that are selected for the final design of the OPS film. These boundaries permit the control of the evolution of the surface of the OPSs versus the scattering angle. Thus, the latter allow minimizing and compensating the harmful dependency of the optical probe volume dimension (not relevant to the particle scattering properties) and the anisotropy of the scattering diagrams with the scattering angle. By these means, and for the OPS film shown in Fig. 3(c), the dynamic of the raw scattering diagrams is reduced by a factor  $\approx 1:54$ .

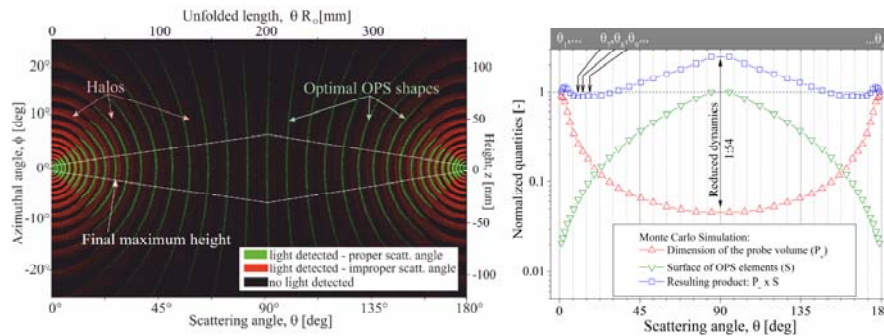


**Fig. 4.** Monte-Carlo simulations: (a) conditional map of light rays passing through (green and red) the optical mask shown in Fig. 3 and that are detected by an OPS film with a virtually infinite spatial resolution. The green regions identify the optimal photosensitive areas that are printed on the OPS film (i.e., OPSs with required angular resolution and no crosstalk). The white lines delimits the upper and lower angular boundaries of the OPSs; (b) evolution with the scattering angle of the probe volume dimension, the surface of the OPSs and the corresponding product (to which the measured optical signals are directly proportional).

#### 4. Numerical and experimental validations

The performance of this design and optimization work is illustrated in Fig. 5 and Table 1. Figure 5(a) compares the LMT and Monte Carlo predictions with experimental scattering diagrams recorded by the prototype in the case of three monosized latex suspensions (from Magsphere Inc. and with a NIST certificate). The certified parameters of these suspensions are summarized in Table 1.

**Table 1. Statistical moments of the PSD of three latex suspensions: certified values (NIST Traceable Standards) and values (i.e. particle size) retrieved with the prototype.**

Sample	Certified values [nm]		Retrieved values [nm]	
	Mean	StD	Mean	StD
(1)	195±5	10	200	10
(2)	770±10	59	780	50
(3)	1000±15	46	990	60

For all experimental tests and calculations reported here a single scattering regime is assumed (i.e., optically dilute suspensions, a typical assumption for most MALS instruments). In the same way, for these preliminary tests, and notably the inversion procedure, the suspensions are simply characterized by a particle relative refractive index  $m \approx 1.2$  and a Particle-Size Distribution (PSD). Note that in the single scattering regime, the particle concentration just acts as a scalar multiplication factor of the scattering diagrams (e.g., [1]).

The PSD is assumed to be a normal distribution depending only on the mean diameter,  $\bar{D}$ , and the corresponding standard deviation,  $\sigma_D$ . Its boundaries  $\{D_{\min}, D_{\max}\}$  are set at 1/1000 of the PSD maximum. So that the first two statistical moments of the PSDs can be deduced from a simple non-negativity-constrained least squares algorithm and a  $\chi^2$  test [19]. To do so, step increments of 10 nm and 5 nm are used for the mean diameter and the standard deviation respectively. Classically [1], a fourth certified latex particle suspension (with  $\bar{D}=20$  nm and  $\sigma_D \approx 1-5$  nm) is used to calibrate the probe volume variations with the scattering angle as well as the electronic gain of all OPS channels, and most (but not all) effects of specular reflection. Note that Monte Carlo simulations are normalized in the same way (latex suspension of 20 nm, etc.) in order to be compared to experimental data and LMT predictions. For the experimental angular calibration of the system, and since all OPSs are auto-aligned on the OPS film, only one calibration point with a precision goniometer is necessary.

Fig. 5(a) shows that the Monte Carlo simulations agree well with the experimental data (time averaged over 100 acquisitions, i.e.  $\approx 1$  seconds). The LMT predictions are also rather convincing in the near-forward and sideways scattering regions. However, as expected, in the backward domain, the experimental and Monte Carlo scattering diagrams are totally polluted by false reflections (i.e. essentially the diffraction of the sample that is partly reflected back by the cuvette). Note that due to some unexpected technical limitations, the first two and last two OPSs ( $j=1, 2, 39$  and  $40$ ) were not working properly. To conclude on that point, when the LMT is used as the scattering model, only the experimental data within the range  $\theta \approx 2-120^\circ$  could be used for the inversion step. By doing so, the statistical moments retrieved for these three suspensions are shown in Table. 1, while Fig. 5(b) shows the corresponding PSDs. Within the experimental uncertainties, these values are consistent with the certified ones.

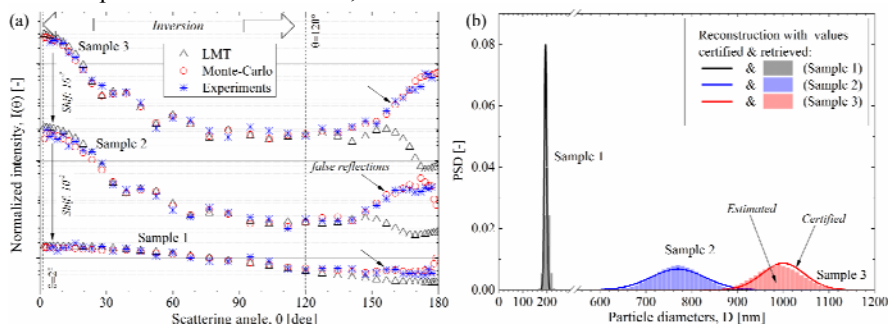


**Fig. 5.** (a) Comparison of the LMT and the Monte Carlo simulations with the time averaged experimental scattering diagrams recorded for three latex suspensions and the perpendicular polarization. For clarity, the scattering diagrams of samples 1 and 2 are shifted in intensity; (b) Illustration of the PSDs retrieved with the prototype with those reconstructed with certified values.

## 5. Conclusion

In summary, this article reports the first implementation of a MALS system that is based on the emerging and rapidly developing OPS technology. The preliminary numerical and experimental results reported here clearly demonstrate the potential of this technology for the characterization of particle systems. It is believed that the ability of this technology to produce on demand conformable films with self-auto-aligned and arbitrarily-shaped photosensitive arrays makes it a unique tool, opening up new perspectives for the characterization of suspensions as well as aerosols and complex shaped particles (e.g. [2, 5, 9, 19-21]). The optimization and various developed models will be detailed in a forthcoming work.

## Acknowledgments.

The authors would like to thank Stéphane Martinez and Sadi Noel for their technical support and assistance, and Bpifrance (project: OptiPAT, OSEO-AAP-FUI12) and the French

Matthias Sentis, Fabrice R.A. Onofri, Olivier Dhez, Jean-Yves Laurent, and Fabien Chauchard, "Organic photo sensors for multi-angle light scattering characterization of particle systems," *Opt. Express* **23**, 27536-27541 (2015) <https://doi.org/10.1364/OE.23.027536>

National Research Agency (project: Nanomorph, ANR-13-BS09-0008-01) for their financial support.